




Martian Thermosphere Response to Solar Flares: MAVEN NGIMS Observations

Zi-Chuan Li^{1,2} and Yu-Tian Cao³ 

¹ National Astronomical Observatories, Chinese Academy of Sciences, Beijing 100101, China

² School of Astronomy and Space Science, University of Chinese Academy of Sciences, Beijing 100049, China

³ Planetary Environmental and Astrobiological Research Laboratory (PEARL), School of Atmospheric Sciences, Sun Yat-Sen University, Zhuhai 519082, China; caoyt6@mail.sysu.edu.cn

Received 2023 March 6; revised 2023 March 20; accepted 2023 March 27; published 2023 April 26

Abstract

The solar flare is a sudden eruptive solar phenomenon with significant enhancements in solar X-ray and Extreme Ultraviolet radiations, resulting in large amounts of energy being injected into the planetary atmosphere. Case studies have been extensively presented to analyze the effect of extremely large flares on the Martian upper atmosphere, but the general features of the Martian thermospheric response to flares are still poorly understood. In this work, we select 12 intense solar flares that occurred between 2015 and 2017 and investigate the densities and compositional variations of the dayside Martian thermosphere to these flares with the aid of the measurements made by the Mars Atmosphere and Volatile Evolution. The statistical studies indicate that the responses of the Martian thermosphere to flares are complicated that both the class of the flare and the wavelength of the enhanced radiation may have prominent influences on the thermal expansion of the atmosphere and the atmospheric photochemical reactions.

Key words: Sun: flares – planets and satellites: atmospheres – planets and satellites: individual (Mars)

1. Introduction

The Martian thermosphere is the transition region from a well-mixed lower atmosphere (mesosphere) to regions where gases diffusively separate and are lost to space (exosphere) (e.g., Bougher et al. 2015, 2017). The characteristics of the Martian thermosphere have been extensively studied since the dawn of the space age, with missions such as the Marine 6, 7, and 9 (Barth et al. 1971, 1972; Stewart 1972; Stewart et al. 1972), Viking Landers 1 and 2 (Nier & McElroy 1977), Mars Global Surveyor (Keating et al. 1998), Mars Express (MEX) (Forget et al. 2009; McDunn et al. 2010), and more recently the Mars Atmosphere and Volatile Evolution (MAVEN) (Jakosky et al. 2015). In addition to the in situ and remote measurements, a new Mars Global Ionosphere-Thermosphere Model (MGITM) is developed to accurately describe the features of the compositional and thermal structure of the Martian thermosphere (Bougher et al. 2015). Observations and simulations have revealed that the structure and circulation of this region were driven both by energy and momentum fluxes from the lower atmosphere and by solar X-ray/Extreme Ultraviolet (EUV) radiation, solar energetic particle as well as solar wind influx from above (e.g., Bougher 1995; Krasnopolsky 2002; Bougher et al. 2015; Nagaraja & Chakravarty 2022; Wu et al. 2022).

The solar flare is a unique driver among the external drivers of Martian thermospheric variability. It is a sudden eruptive solar phenomenon with significant enhancements in X-ray and EUV

radiations, resulting in amounts of energy injection into the planetary atmosphere (Wang et al. 2007). According to the peak flux measured in the 0.1–0.8 nm wavelength band, solar flares are often ranked from weak to intense as C-class for Common flare, M-class for moderate flare, and X-class for extreme flare (Yashiro et al. 2006). The effects of solar flares on the Earth's thermosphere have been widely studied. For instance, Le et al. (2012) analyzed the neutral density of the earth's thermosphere response to all X-class solar flares from 2001 to 2006. The observations revealed that X5 and stronger solar flares can cause an average 10%–13% increase in thermospheric density at low to middle latitudes within 4 hr of onset. They discovered that thermospheric density enhancement was much more dependent on integrated EUV flux than peak EUV or X-ray flux, with a correlation coefficient of 0.91. Pawlowski & Ridley (2008) used the Global Ionosphere-Thermosphere Model (GITM) to simulate the global thermospheric responses to the solar flares on 2003 October 28, and 2004 November 6, respectively. According to the model, the thermospheric density at 400 km was increased by a maximum of 14.6% within 2 hr of the flare's onset and took 12 hr to return to normal. They found that flare-induced dayside heating could cause nightward propagating gravity waves, resulting in nightside atmospheric perturbations.

Compared with the Earth's atmosphere, the Martian atmosphere is relatively tenuous with a smaller optical depth and is expected to respond faster and be more sensitive to solar

flares. Gurnett et al. (2005) reported the first experimental evidence of Martian atmospheric responses to solar flares. They found that the surface reflections detected by Mars Advanced Radar for Subsurface and Ionosphere Sounding (MARSIS) on board the MEX disappeared completely about 2 days after the X17 solar flare of 2005 September 7, implying that the Martian ionosphere was disturbed by energetic charged particles produced by solar flares, resulting in the enhanced absorption of radio waves in the lower level of the ionosphere. Mendillo et al. (2006) reported the responses of solar flares that caused enhancements to the ionosphere of Mars as reported by the Mars Global Surveyor (MGS). They found a 200% increase in the E-region electron density due to solar flares of 2001 April 15 and 26. Later Haider et al. (2009) identified a 150% increase in the E-region electron density due to the solar flare of 2005 May 13. Lollo et al. (2012) modeled the electron density profiles of 2001 April 15 and 26. They found that the E-peak density can exceed the F-peak during intense solar flares.

The effects of solar flares on the Martian thermosphere, particularly for neutral species, were poorly constrained by observations until the MAVEN arrived in 2014. MAVEN carries instruments that can simultaneously measure the solar X-ray/EUV flux at Mars and the Martian thermospheric neutral densities, allowing us to investigate the Martian thermospheric response to solar flares. With the aid of the solar X-ray/EUV flux measured by the Extreme Ultraviolet Monitor (EUVM) and the atomic Ar density measured by the Neutral Gas and Ion Mass Spectrometer (NGIMS) onboard MAVEN, Thiemann et al. (2015) examined the thermospheric temperature variation caused by 14 M-class or greater solar flares occurred from 2014 October to 2015 May. They reported that the dayside thermosphere showed significant heating near the flare soft X-ray peak, and responded and recovered rapidly. Focusing on an intense flare that occurred on 2017 September 10 with X8.2 class, Cramer et al. (2020) reported the solar flare effect on the density and composition of the Martian thermosphere. They found that at fixed altitudes, the number densities of all species barring the atomic Helium increased significantly, while the O/CO₂ ratio decreased by 1545%. When viewed at fixed total number densities, the densities of CO₂ and Ar decreased, and the O/CO₂ ratio increased by up to a factor of 3. Fang et al. (2019) further simulated the global and time-dependent Martian thermospheric responses to this solar flare, and reported that the neutral atmospheric perturbation took 2.5 hr after the flare peak to reach the maximum density enhancement and another 10 hr to return to pre-flare levels.

Response to the extremely large flare, such as the X8.2 flare in 2017, has been well studied, but the general features of the Martian thermospheric response to flares are still poorly understood, which serves as the main motivation of the present study. Based on the MAVEN data sets, we select 12 M-class or great flares that occurred between 2015 and 2017 and analyze the response of the Martian thermosphere. The layout of the

paper is as follows. A brief description of the MAVEN data sets and the methodology used for the study are provided in Section 2. We then present in Section 3 the responses of the thermosphere to the different solar flares, including the densities of different neutral species, and the variation of the density ratio between O and CO₂. The implications of these observations and the effect of solar flares on the Martian thermosphere are discussed in Section 4, followed by the concluding remarks in Section 5.

2. Dataset and Methodology

MAVEN has been orbiting Mars since 2014 September, using nine onboard science instruments to investigate the interactions of the Sun and solar wind with the Martian magnetosphere and upper atmosphere (Jakosky et al. 2015). It has a highly eccentric orbit with periapsis near 150 km and apoapsis near 6200 km within a 4.5 hr period.

Densities of neutral species used in this study are provided by the MAVEN NGIMS instrument (Mahaffy et al. 2015). The NGIMS is a quadrupole mass spectrometer capable of measuring accurate density profiles of various constituents of the Martian neutral atmosphere from periapsis (~150-160 km for nominal science operations) to ~300 km. Individual measurements are taken every 2 s during a 20 minutes collection period for each periapsis pass.

Solar X-ray/EUV flux incident at Mars is provided by the MAVEN EUVM instrument (Eparvier et al. 2015). The EUVM instrument continuously monitors the solar X-ray/EUV flux across three wavelength channels: 0–7 nm, 17–22 nm, and 117–125 nm. The full solar spectrum up to 190 nm is constructed using the EUVM band irradiance data and the Flare Irradiance Spectral Model-Mars (FISM-M), with a 1 nm wavelength resolution at a cadence of 1 minute. The EUVM Level 2 data product contains the irradiance of the three channels, while the Level 3 data product contains the modeled spectral irradiance variability at Mars.

To select the flare-affected neutral density profiles from NGIMS data sets, we use the following criteria: (1) the flare event was identified by the Geostationary Operational Environmental Satellites (GOES, <https://www.ngdc.noaa.gov/stp/solar/solarflares.html>) (Liu et al. 2017) and was observed by EUVM at Mars simultaneously, (2) NGIMS measured the atmosphere density during the flare period, which requires the spacecraft to pass by the periapsis during the flare period, and (3) the orbit periapsis occurred on the dayside of Mars, which requires the solar zenith angle (SZA) of the orbit near the periapsis below 90°. In addition, we rule out the observations during the solar energetic particle (SEP) events and the global dust storm, which may strongly affect the thermosphere as well (e.g., Leblanc et al. 2002; Niu et al. 2021). The SEP event can be identified by the SEP instrument onboard MAVEN (Larson et al. 2015), and the global dust storm can be identified by the

Table 1
NGIMS Measurements Coincided with Solar Flares at Mars

Number	Flare Peak Time	Class	Peak X-Ray ^a (mW m ⁻²)	Duration (hr)	Flare Orbit	Delay ^b (hr)	Periapsis SZA (deg)	Response Type ^c
1	1/3/2015 12:44	X1.2	3.9	1.5	811	1.8	86	III
2	7/3/2015 22:32	M8.9	3.2	3.7	845	1.32	75	III
3	21/3/2015 7:47	M1.1	>0.9	0.4	916	0.35	53	III
4	24/3/2015 8:48	M3.0	>1.7	0.3	932	-0.43	49	II
5	4/5/2015 12:07	M1.1	1.0	0.9	1152	0.38	22	III
6	21/5/2015 22:30	M1.3	1.0	0.6	1246	0.38	48	II
7	30/9/2015 11:14	M1.0	0.7	0.7	1951	0.68	68	II
8	7/9/2017 16:00	X1.3	>0.3	3.2	5702	2.75	73	I
9	8/9/2017 7:50	M8.1	>0.5	2.8	5705	0.22	72	III
10	8/9/2017 16:02	M2.9	0.6	1.4	5707	0.88	72	I
11	10/9/2017 16:06	X8.2	9.0	3.4	5718	1.6	70	I
12	17/9/2017 12:10	M6.0	1.1	9.3	5755	1.6	63	III

Notes.

^a MAVEN EUVM solar irradiance measured at the flare peak for the X-ray (0–7 nm) band. For flares 3, 4, 8 and 9, these flares were not fully observed throughout the flare periods, and the observed maximum fluxes are used to represent the flux peaks.

^b Difference between periapsis and flare peak times. The negative sign indicates that the periapsis time is earlier than the flare peak time.

^c The types of the thermosphere responses to solar flares, further explained in Section 3.

Mars Climate Sounder on board the Mars Reconnaissance Orbiter (McCleese et al. 2007).

We present in Table 1 the information of the selected flare orbits and the corresponding solar flares. The selected 12 events all happened from 2015 to 2017. Several flare events that happened in 2014 are neglected due to a lack of NGIMS CO and O measurements, particularly because atom O is the dominant species in the Martian thermosphere at altitudes above ~250 km (e.g., Mahaffy et al. 2015).

In this work, we investigate the number densities of five neutral species provided in the NGIMS data, including O, N₂, CO, Ar, and CO₂. Helium is excluded due to the large uncertainty at high altitudes, and only the inbound portion is used to avoid contamination from heterogeneous chemistry and physical adsorption and desorption on the instrument ante-chamber walls (Mahaffy et al. 2015). The density profile of each species is first fitted by a third-order polynomial to remove the disturbance from the possible gravity wave (e.g., Yiğit et al. 2015; Siddle et al. 2019). For each flare event, we select five orbits surrounding the flare orbit and determine the average density profile of these orbits as a representation of baseline atmospheric conditions and the standard deviation of these orbits is thought to be the density variation caused by other factors, such as waves, tides, and longitudinal variations.

In Figure 1, we present the intensity of the solar X-ray radiation over the wavelength range of 0–7 nm of the selected 12 cases. The peak intensity during a flare measured by EUVM is shown as the red solid circle. It is notable that EUVM did not observe the peak structure in the intensities of cases 3, 4, 8, and 9. The peak intensities of these four cases are, therefore, defined as the maximum intensity measured by EUVM. The

orange triangle indicates the X-ray intensity measured at the periapsis of the flare orbit, and the gray inverted triangle indicates the mean value of the intensities measured at the periapsis of the orbits used in determining the baseline.

3. Results

To characterize the Martian thermosphere responses to solar flares, we analyze first the total neutral densities, summed over O, N₂, CO, Ar, and CO₂, of the flare orbits and the corresponding baselines below 250 km. At each altitude, if the total number density for the flare orbit is larger than its baseline value and exceeds the average by over one standard deviation, the response is defined as effectively enhanced. According to the responses of total density profiles to the flares, we categorize the 12 flare events into three types. Type I includes the cases that the over 65% of the data points are enhanced effectively, Type II includes the cases that the effectively enhanced data points that take up between 65% and 35%, and Type III includes the cases that less than 35% of the data points are enhanced effectively. The type of each flare is listed in the right-most column in Table 1. For illustrative purposes, we present in Figure 2 the total number density profiles of three cases as the representative of three types of response. In each panel, the dashed line and solid line indicate the density profile of the flare orbit and the baseline, respectively. Error bars for the solid line are derived from the standard deviation of the densities from the set of baseline orbits for each altitude.

In the left panel of Figure 2, we present the density profile of flare 11, the X8.2 class flare that happened on 2017 September

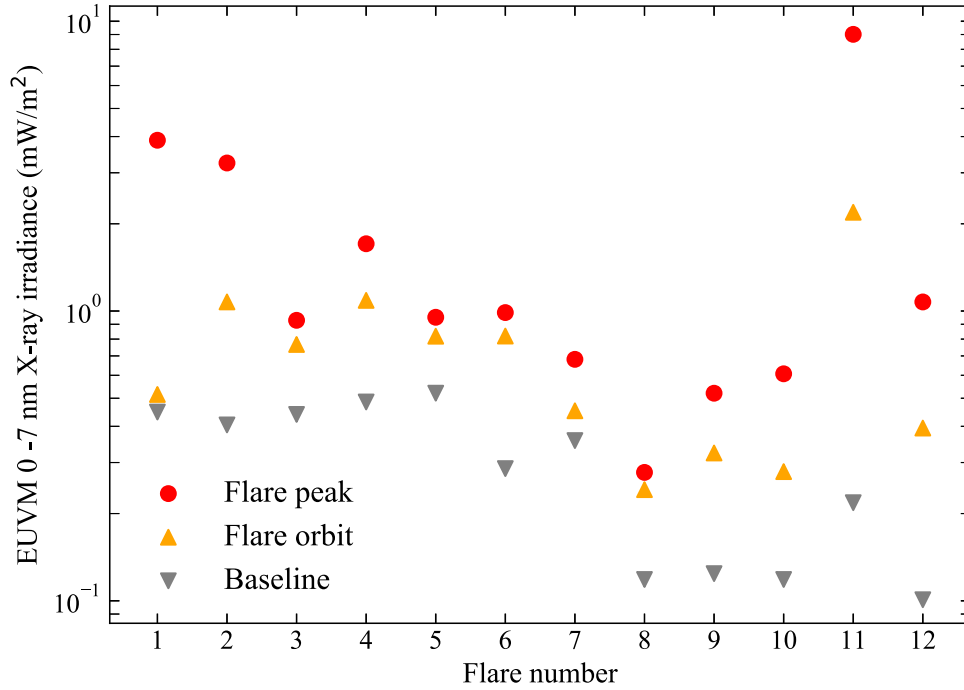


Figure 1. MAVEN EUVM solar X-ray (0–7 nm) band fluxes of the 12 solar flares. For each solar flare, the flux of the flare peak, as well as the mean flux during the periapsis segment of the flare orbit and the baseline orbits, are marked in different ways.

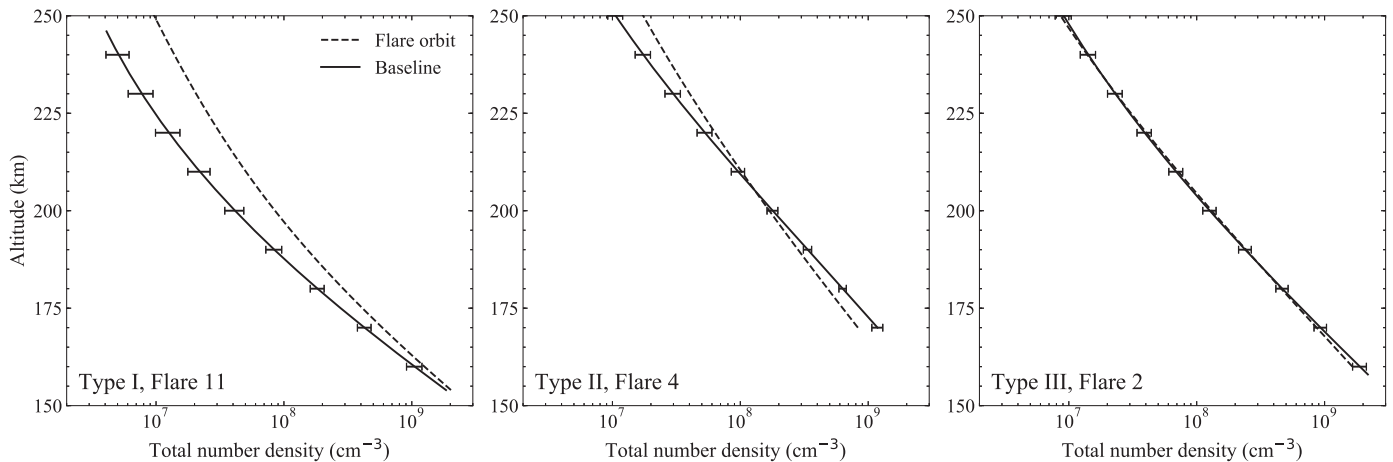


Figure 2. The total number density profiles of three cases, as representative of three types of response. The dashed line and solid line indicate the density profile of the flare orbit and the baseline, respectively. Error bars for the solid line are derived from the standard deviation of the densities from the set of baseline orbits for each altitude.

10 and has been extensively studied (e.g., Fang et al. 2019; Cramer et al. 2020). Compared with the baseline, the total number density of the flare orbit enhanced by 9% at a periapsis of 152 km and the enhancement increased prominently with the altitude. The middle panel shows the density profile of flare 4, a M3.0 class flare that happened on 2015 March 24. The total number density of flare 4 is reduced than the density of the baseline below 206 km and the density of flare 4 is only 70% of

the baseline density at a periapsis of 170 km. However, the density of flare 4 decreased slowly with the increasing altitude, compared with the baseline density variation and the density of flare 4 increased to 165% of the baseline density at 250 km. The right panel presents the density profile of flare 2, a M8.9 class flare that happened on 2015 March 7, during which the densities of the flare orbit and the baseline are almost identical at all altitudes.

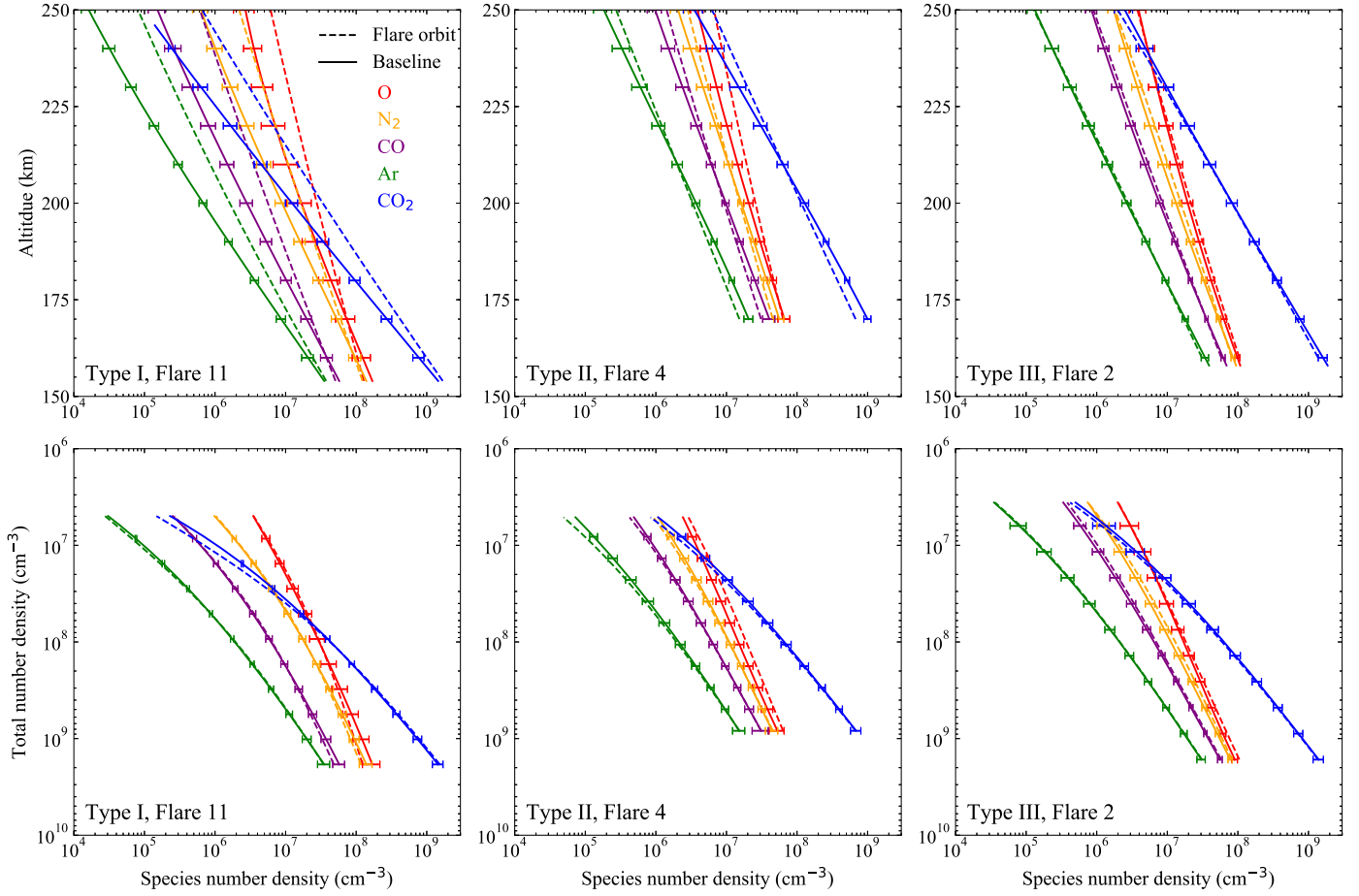


Figure 3. (Top) The dependence of the densities of five neutral species (O, N₂, CO, Ar, and CO₂) on altitude for the flare orbit and the baseline for the three representative cases. (Bottom) The dependence of the densities of the same five neutral species on the total number density for the flare orbit and the baseline for the three representative cases.

Because the dominant species of Martian thermosphere changes from CO₂ below ~ 250 km to O at higher altitudes, we present in the upper row of Figure 3 the dependence of the densities of five neutral species (O, N₂, CO, Ar, and CO₂) on altitude for the flare orbit and the baseline for the three cases discussed above. For flare 11, all five species show prominent enhancement at all altitudes during the flare, in agreement with prior studies of the thermosphere response to this flare (e.g., Fang et al. 2019; Cramer et al. 2020). For flare 4, the studied species barring atomic oxygen show a similar tendency to the total number density in Figure 2 that below ~ 220 km the densities of the flare orbit are significantly reduced than the baseline densities and become larger than the baseline densities at higher altitudes. The abundance of O is notably larger for the flare 4 orbit than its baseline value at all altitudes and exceeds the average by more than one standard deviation at altitudes above 190 km. The densities of all five species for flare 2 are also nearly identical to its baseline value.

The aforementioned results focus on the dependence of the density on altitude, which may be caused both by the thermal expansion of the bulk atmosphere and by chemical changes in atmospheric composition. We, therefore, use total number density as a proxy for pressure and present the density dependence of each species on the total number density to exclude the contribution of thermal expansion. The bottom row of Figure 3 shows the same number density profiles of individual species as the upper row for three cases but expressed relative to total number density rather than altitude. Changes in the species number densities with respect to the total number density during the flare orbit appear significantly smaller than the changes of number densities with respect to the altitude for all species and for all the three cases, except O during flare 4. The abundance of O is prominently larger for the flare 4 orbit than its baseline value and exceeds the average by more than one standard deviation.

In addition to the number density of different species, the O/CO₂ density ratio is also an important indicator that provides

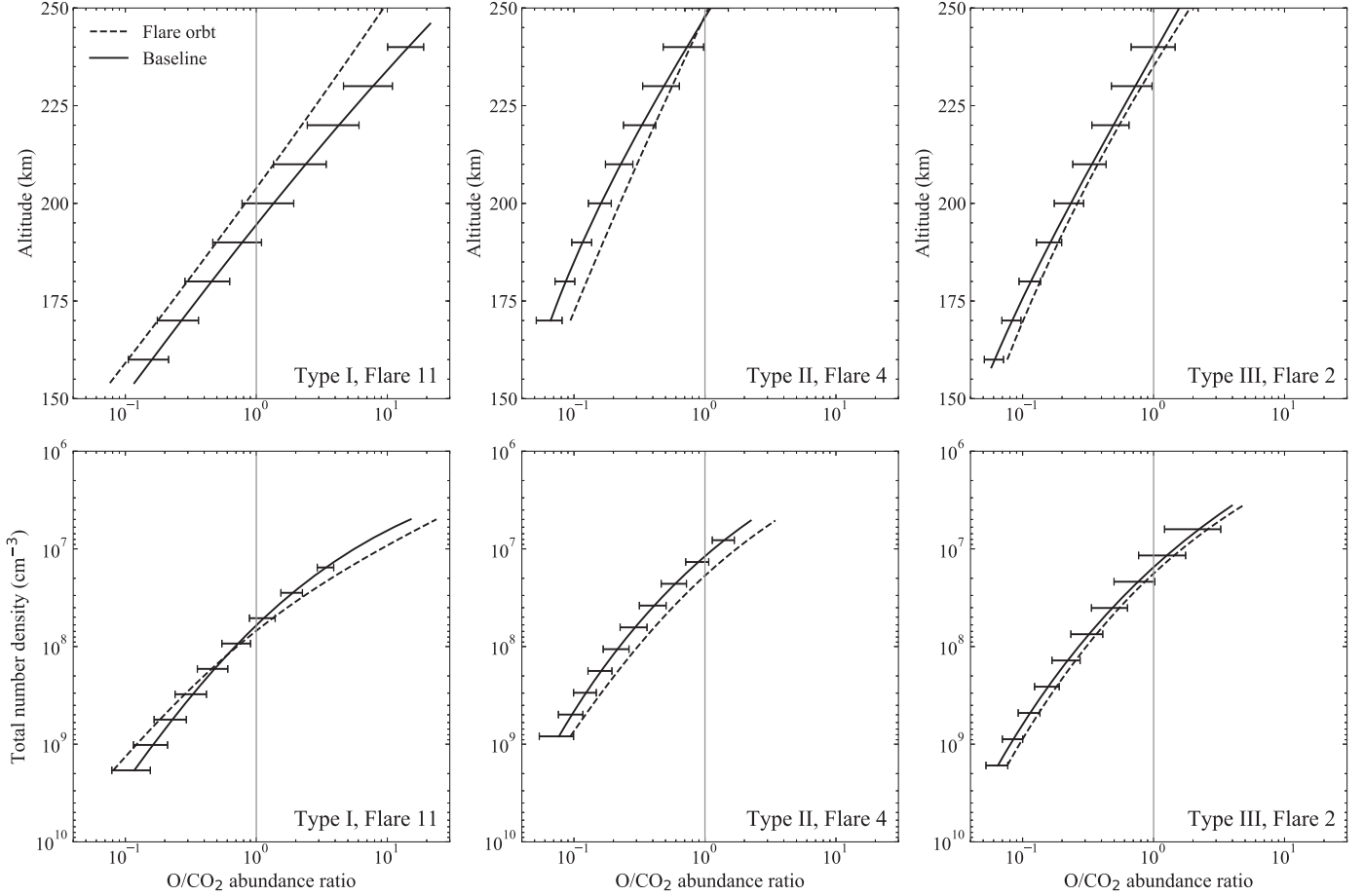


Figure 4. (Top) The dependence of the O/CO₂ density ratio on altitude, in the same format as in Figure 2, with the vertical solid line indicating that CO₂ density equals O density. (Bottom) The dependence of the O/CO₂ density ratio on the total number density.

information on the Martian thermosphere because CO₂ and O are the most abundant species in the lower and upper altitudes of the thermosphere, respectively. We, therefore, provide in Figure 4 the variation of the O/CO₂ density ratio for three cases with respect to altitude and total number density, respectively. The upper row of Figures presents the dependence of the O/CO₂ density ratio on altitude, in the same format as in Figure 2, with the vertical solid line indicating that CO₂ density equals O density.

For flare 11, the O/CO₂ density ratio of the flare orbit is smaller than the value of the baseline at all altitudes. The altitude where CO₂ density equals O density increases from 195 km for baseline to 204 km during the flare orbit. The situation for flare 4 is quite different in that the O/CO₂ density ratio of flare orbit is larger than the value of the baseline at all altitudes and the altitudes where CO₂ density equals O density are both 250 km for both flare 4 orbit and its baseline. For flare 2, in which the number density shows little changes between the flare orbit and its baseline, the O/CO₂ density ratio of the flare orbit is also larger than the value of the baseline at all

altitudes. However, the differences are only limited to one standard deviation at altitudes above 170 km.

We also provide in the bottom row of Figure 4 the dependence of the O/CO₂ density ratio on the total number density. The O/CO₂ density ratio of flare 11 orbit is 69% of the O/CO₂ density ratio of the baseline when the total number density is $1.9 \times 10^9 \text{ cm}^{-3}$. With the total number density decreasing, the O/CO₂ density ratio of flare 11 orbit increases faster than the increase of the O/CO₂ density ratio of the baseline. The O/CO₂ density ratio of flare 11 orbit equals the O/CO₂ density ratio of the baseline when the total number density reaches $1.2 \times 10^8 \text{ cm}^{-3}$. When the CO₂ density equals O density, the total number density of flare 4 orbit is $1.9 \times 10^7 \text{ cm}^{-3}$, larger than its baseline value of $1.2 \times 10^7 \text{ cm}^{-3}$, but the corresponding altitude of the flare 4 orbit is identical to the altitude of the baseline. Changes in O/CO₂ density ratio with respect to the total number density during the flare orbit is as weak as the changes of O/CO₂ density ratio with respect to the altitude for flare 2.

4. Discussions

In order to investigate the response of the Martian thermosphere to the solar flare, we analyze 12 M-class or greater flares that MAVEN observed the enhanced X-ray radiation and measured the thermospheric neutral densities simultaneously. The apparent responses of species densities and atmospheric composition to solar flares indicate that the response of the Martian thermosphere to the solar flares is complicated. For flares as strong as the X8.2 class flare that happened on 2017 September 10, the neutral density of the thermosphere is enhanced prominently at all altitudes. The species number densities with respect to the total number density, however, change slightly during this flare orbit compared with the baseline. The result indicates that the flare mainly leads to the thermal expansion of the bulk atmosphere, and the photochemical changes in the atmospheric composition are weakly affected.

For a weaker flare of M3.0 class happened on 2015 March 24, the number density of CO₂, N₂, CO, and Ar enhanced only at altitudes above 210 km, compared to the baseline. The density of the atomic oxygen, however, is enhanced at all altitudes. The density variations are more obvious with respect to the total number density that the number density of O during the flare orbit is prominently increased than that of the baseline, exceeding the average by over one standard deviation over the density range of $\sim 10^7$ – 10^9 cm⁻³. A larger O/CO₂ density ratio during the flare orbit compared with the value of its baseline further indicates that during this flare event the photochemical reactions are enhanced but the thermal expansion of the bulk atmosphere is weak.

However, during the M8.9 class flare that happened on 2015 March 7, which should be significantly stronger than the M3.0 class flare discussed above, no obvious changes in the thermosphere have been observed, neither for number densities nor for atmospheric compositions. A 1.32 hr delay and a high SZA of 75° of the observation may contribute to this weak response. Without showing details, we mention that for flare 5, in which MAVEN measured the thermosphere 0.38 hr after the flare peak at an SZA of 22°, only a slight response of the thermosphere is recorded because the flare is as weak as M1.0 class.

Our statistical results indicate that the responses of the Martian thermosphere to flares are not only related to the intensity of the flare, but are also affected by the time delay and the position, such as the SZA. Fang et al. (2019) also reported that the solar flare effectiveness in the neutral atmosphere proceeds through an accumulation and redistribution process, which naturally results in a much longer reaction time compared to the electrons and ions. In addition, the solar flares are often ranked according to the peak flux measured in the 0.1–0.8 nm, corresponding to the soft X-ray band, and the photoabsorption cross section of CO₂ over this wavelength

range is smaller than the photoabsorption cross section over the EUV band (Huestis & Berkowitz 2010). Therefore, an intense solar flare may not result in the increase of photochemical reaction rate in the Martian thermosphere, if only the X-ray radiation is increased during this flare. The strong X-ray radiation is more likely to penetrate to the lower atmosphere and leads to a thermal expansion of the bulk atmosphere. Sometimes, however, a weak solar flare may have a prominent increase in EUV radiation, which can strongly increase the photochemical changes in the thermosphere and result in a strong response of the atmospheric compositions at high altitudes.

5. Conclusions

Solar flares are transient events that release a tremendous amount of energy and impose significant disturbances upon planetary atmospheres. In order to investigate the response of the Martian thermosphere to the solar flare, we analyze 12 M-class or greater flares based on the MAVEN EUVM observations of the enhanced X-ray radiation and the NGIMS observations of the neutral density of the Martian thermosphere simultaneously. The response of the Martian thermosphere can be generally categorized into three types. For the first type, the neutral density of the thermosphere is enhanced prominently at all altitudes during the flare event, due to the thermal expansion of the bulk atmosphere. For the second type, the neutral density of the thermosphere is enhanced only at high altitudes, particularly for the atomic oxygen. This response may be caused by the enhancement of the photochemical changes resulting from the solar flare. In addition to the strong response, the Martian thermosphere changes slightly during some flares, as the third type of response, which can be observed during both intense and weak flare events.

Our statistical results indicate that the responses of the Martian thermosphere to flares are so complicated that both the class of the flare and the wavelength of the enhanced radiation have an influence on the Martian thermosphere. In addition, the solar flare effectiveness in the neutral atmosphere proceeds through an accumulation and redistribution process, and the observed of the thermospheric response is, therefore, affected by the time delay and the location of the measurements. The work presented here serves both to confirm the results of previous studies, as well as to act as a foundation for future studies on the response of the Martian upper atmosphere to solar flares.

Acknowledgments

This work is supported by the Guangdong Basic and Applied Research Foundation through Grant 2021A1515110271.

ORCID iDsYu-Tian Cao  <https://orcid.org/0000-0003-0858-4488>**References**

- Barth, C. A., Hord, C. W., Pearce, J. B., et al. 1971, *JGR*, **76**, 2213
- Barth, C. A., Stewart, A. I., Hord, C. W., & Lane, A. L. 1972, *Icarus*, **17**, 457
- Bougher, S. W. 1995, *AdSpR*, **15**, 21
- Bougher, S. W., Brain, D. A., Fox, J. L., et al. 2017, Upper neutral atmosphere and ionosphere, *The Atmosphere and Climate of Mars* (Cambridge: Cambridge Univ. Press), 405
- Bougher, S. W., Pawlowski, D., Bell, J. M., et al. 2015, *JGRE*, **120**, 311
- Cramer, A. G., Withers, P., Elrod, M. K., Benna, M., & Mahaffy, P. R. 2020, *JGRA*, **125**, e28518
- Eparvier, F. G., Chamberlin, P. C., Woods, T. N., & Thiemann, E. M. B. 2015, *SSRv*, **195**, 293
- Fang, X., Pawlowski, D., Ma, Y., et al. 2019, *GeoRL*, **46**, 9334
- Forget, F., Montmessin, F., Bertaux, J.-L., et al. 2009, *JGRE*, **114**, E01004
- Gurnett, D. A., Kirchner, D. L., Huff, R. L., et al. 2005, *Sci*, **310**, 1929
- Haider, S. A., Abdu, M. A., Batista, I. S., et al. 2009, *GeoRL*, **36**, L13104
- Huestis, D. L., & Berkowitz, J. 2010, AAS/DPS Meeting Abstracts, **42**, 48.13
- Jakosky, B. M., Lin, R. P., Grebowsky, J. M., et al. 2015, *SSRv*, **195**, 3
- Keating, G. M., Bougher, S. W., Zurek, R. W., et al. 1998, *Sci*, **279**, 1672
- Krasnopolsky, V. A. 2002, *JGRE*, **107**, 5128
- Larson, D. E., Lillis, R. J., Lee, C. O., et al. 2015, *SSRv*, **195**, 153
- Le, H., Liu, L., & Wan, W. 2012, *JGRA*, **117**, A03307
- Leblanc, F., Luhmann, J. G., Johnson, R. E., & Chassefiere, E. 2002, *JGRA*, **107**, 1058
- Liu, J.-F., Li, F., Zhang, H.-P., & Yu, D.-R. 2017, *RAA*, **17**, 116
- Lollo, A., Withers, P., Fallows, K., et al. 2012, *JGRA*, **117**, A05314
- Mahaffy, P. R., Benna, M., King, T., et al. 2015, *SSRv*, **195**, 49
- McCleese, D. J., Schofield, J. T., Taylor, F. W., et al. 2007, *JGRE*, **112**, E05S06
- McDunn, T. L., Bougher, S. W., Murphy, J., et al. 2010, *Icarus*, **206**, 5
- Mendillo, M., Withers, P., Hinson, D., Rishbeth, H., & Reinisch, B. 2006, *Sci*, **311**, 1135
- Nagaraja, K., & Chakravarty, S. C. 2022, arXiv:2210.01417
- Nier, A. O., & McElroy, M. B. 1977, *JGR*, **82**, 4341
- Niu, D. D., Cui, J., Wu, S. Q., et al. 2021, *JGRE*, **126**, e06679
- Pawlowski, D. J., & Ridley, A. J. 2008, *JGRA*, **113**, A10309
- Siddle, A. G., Mueller-Wodarg, I. C. F., Stone, S. W., & Yelle, R. V. 2019, *Icarus*, **333**, 12
- Stewart, A. I. 1972, *JGR*, **77**, 54
- Stewart, A. I., Barth, C. A., Hord, C. W., & Lane, A. L. 1972, *Icarus*, **17**, 469
- Thiemann, E. M. B., Eparvier, F. G., Andersson, L. A., et al. 2015, *GeoRL*, **42**, 8986
- Wang, L., Fang, C., & Ding, M.-D. 2007, *ChJAA*, **7**, 721
- Wu, Z., Li, T., Heavens, N. G., et al. 2022, *ESRv*, **229**, 104023
- Yashiro, S., Akiyama, S., Gopalswamy, N., & Howard, R. A. 2006, *ApJL*, **650**, L143
- Yiğit, E., England, S. L., Liu, G., et al. 2015, *GeoRL*, **42**, 8993